IEEE Access
Multidisciplinary ⋮ Rapid Review ⋮ Open Access Journal

Received 18 July 2023, accepted 24 September 2023, date of current version 16 October 2023.

Digital Object Identifier 10.1109/ACCESS.2023.3322376

RESEARCH ARTICLE

Sparrow Search Algorithm With Stacked Deep Learning Based Medical Image Analysis for Pancreatic Cancer Detection and Classification

JANJHYAM VENKATA NAGA RAMESH[1], T. ABIRAMI[2], T. GOPALAKRISHNAN[3], (Member, IEEE), KANAGARAJ NARAYANASAMY[4], (Member, IEEE), MOHAMAD KHAIRI ISHAK[5,6], FATEN KHALID KARIM[7], SAMIH M. MOSTAFA[8,9], AND ALAA ALLAKANY[10]

[1]Department of Computer Science and Engineering, Koneru Lakshmaiah Education Foundation, Vaddeswaram, Vijayawada, Andhra Pradesh 522502, India
[2]Department of Information Technology, Kongu Engineering College, Erode 638060, India
[3]Department of Information Technology, Manipal Institute of Technology Bengaluru, Manipal Academy of Higher Education, Manipal 576104, India
[4]Department of Computer Science, Karpagam Academy of Higher Education, Coimbatore 641021, India
[5]School of Electrical and Electronic Engineering, Engineering Campus, Universiti Sains Malaysia, Nibong Tebal 14300, Malaysia
[6]Department of Electrical and Computer Engineering, Ajman University, Ajman, United Arab Emirates
[7]Department of Computer Sciences, College of Computer and Information Sciences, Princess Nourah bint Abdulrahman University, Riyadh 11671, Saudi Arabia
[8]Computer Science Department, Faculty of Computers and Information, South Valley University, Qena 83523, Egypt
[9]Faculty of Industry and Energy Technology, New Assiut Technological University (NATU), New Asyut 71515, Egypt
[10]Faculty of Computers and Information, Kafrelsheikh University, Kafr El-Shaikh 6860404, Egypt

Corresponding author: Faten Khalid Karim (fkdiaaldin@pnu.edu.sa)

This work was supported by Princess Nourah bint Abdulrahman University Researchers Supporting Project number (PNURSP2023R300), Princess Nourah bint Abdulrahman University, Riyadh, Saudi Arabia.

ABSTRACT Medical image analysis for pancreatic cancer (PC) classification and recognition is a vital domain of research and medical practices. PC is challenging to diagnose and treat; medical imaging approaches aid early diagnosis to analyse and treat, and employ of medical imaging approaches are support early diagnosis, correct analysis, and treatment planning. Computed Tomography (CT) scans are generally utilized to detect and classify PCs. Deep learning (DL) approaches have demonstrated the ability to support the diagnosis and detection of several medical conditions, containing PC. Convolutional Neural Networks (CNNs) are a kind of DL approach generally employed for image analysis that is trained to automatically learn and extract features in medical images. So, this study purposes a new Sparrow Search Algorithm with Stacked Deep Learning based Medical Image Analysis for Pancreatic Cancer Detection and Classification (SSASDL-PCDC) technique on CT images. The purpose of the study is to design an SSASDL-PCDC technique to achieve improved pancreatic cancer detection performance. In addition, the SSASDL-PCDC technique applies Harris Hawks Optimization (HHO) with a densely connected networks (DenseNet) model for the feature extraction process. Moreover, convolutional neural network with bi-directional long short-term memory (CNN-BiLSTM) approach was utilized for PC detection and classification. Furthermore, Sparrow Search Algorithm (SSA) is used to adjust the hyperparameter values of the CNN-BiLSTM technique. To evaluate the effectiveness of the SSASDL-PCDC technique, extensive experiments were executed on a comprehensive database of pancreatic CT images. The simulation outcome value depicted that the SSASDL-PCDC technique with maximum sensitivity of 99.26%, specificity of 99.26%, and accuracy of 99.26%.

INDEX TERMS Pancreatic cancer, computed tomography images, sparrow search algorithm, medical image analysis, cancer diagnosis.

I. INTRODUCTION

Pancreatic cancer (PC) is a major cause of death around the world, with growing incidence. Earlier detection of PC

The associate editor coordinating the review of this manuscript and approving it for publication was Eduardo Rosa-Molinar.

is the most important challenge, as the disease is usually diagnosed at later stages [1]. Patients with earlier-stage disease are cured with the help of radiotherapy, surgery, and chemotherapy. Therefore, an optimum understanding of the risk factor for PC and diagnosis at an earlier stage has tremendous potential to reduce overall mortality and improve patient survival. Compared to other cancer types, the incidence of PC is considerably lower, for example colorectal, lung, and breast cancer [2]. The risk of PC was calculated for a long time based on clinical risk, family history, genetic predisposition, circulating biomarkers, and behavioral factors. Presently, patient with high risk due to cystic lesion of the pancreas or family history or rare inherited pathogenic variant undergoes serial pancreas-directed imaging to diagnose earlier PC [3]. But this patient only accounts for a smaller fraction of those progressing PC, and data on genetic risk factors or family history are not frequently accessible in the overall population. CT is the imaging modality used mainly for the assessment and detection of PC, but the method's diagnostic performance is based on the experience of the radiologist [4]. Moreover, about 40% of tumours that are lesser than 2cm evade detection by CT, underscoring a crucial necessity for novel approaches to improve radiologist interpretation in increasing the sensitivity for the analysis of PC [5].

Artificial intelligence (AI) is a field of computer science offered to produce a novel type of intelligent machine, which respond just like human intelligence [6]. Currently, several research workers attempt to exploit AI in the healthcare sector, involving healthcare, cardiology, oncology, etc. In comparison to conventional biometric techniques, AI has great scalability and flexibility that enables it to be deployed for various tasks [7]. An additional benefit is its capability to join in a wide range of data varieties and understands difficult connections among variables in trainable, flexible manners. AI shows more benefits in processing big data as the computer computing power continues to enhance and scale of medical data continues to expand [8]. In medical practice, AI can consistently carry out routine tasks, which free up medical doctor time to resolve medical problems. Deep learning (DL) with convolutional neural networks (CNN) showed great promise in the study of medical images. The construction of a neural network (NN) is based on the stack of neurons encompassed of activation function and parameter to combine and feature extraction in the image and established a mechanism that takes the complex connections among diagnosis and images [9]. CNN accomplishes a high accuracy in the imaging diagnosis of different circumstances including liver masses, skin cancer, and diabetic retinopathy. But, the probable usefulness of CNN for the recognition and diagnoses of PC is not been extensively analyzed [10]. PC frequently proposes with ill-defined margins and irregular contours on CT and therefore are often obscure at a previous stage that possesses significant challenges even for the most experienced radiologist.

This study proposes a novel Sparrow Search Algorithm with Stacked DL based Medical Image Analysis for Pancreatic Cancer Detection and Classification (SSASDL-PCDC) technique on CT images. The SSASDL-PCDC technique applies Harris Hawks Optimization (HHO) with a densely connected networks (DenseNet) model for the feature extraction process. Moreover, a convolutional neural network with bi-directional long short-term memory (CNN-BiLSTM) approach was utilized for PC detection and classification. Furthermore, SSA was utilized to alter the hyperparameter values of the CNN-BiLSTM approach. To evaluate the effectiveness of the SSASDL-PCDC system, extensive experiments were performed on a comprehensive dataset of pancreatic CT images.

II. RELATED WORKS

Alves et al. [11] employed a recent DL approach for developing an automatic structure for PDAC recognition, concentrating on smaller lesions. The PDAC is employed for training a nnUnet for automatic cancer recognition and segmentation (nnUnet+T). The 2 extra nnUnet are trained for investigating the effect of anatomy combination: (i) segmentation of the tumor, pancreas, and multiple surrounding anatomical structures (nnUnet+MS), and (ii) segmentation of the tumor and pancreas (nnUnet+TP). Chaithanyadas and King [12] concentrations on the effectual classification and segmentation of PC utilizing DL approach with the subsequent steps of the procedure: (i) The MRI images gathered in reputed clinics were utilized for the analysis method, (ii) primarily, the raw images can be pre-processing by employing boosted anisotropic diffusion filter (BADF) and CLAHE approaches, (iii) additional, the segmentation method isolates the nodules utilizing FCM clustering (DMFCM) approach, (iv) the features exist before removed and chosen by employing HHO-related SVM.

In [13], the DL approach termed as CNN approach was utilized for predicting the pancreas cancer images that are embedded by the process of Gaussian Mixture model (GMM) with the EM method for forecasting the major features in the CT scan and forecasts the percentage of cancer spread from the pancreas with threshold factors obtained as markers. The authors [14] establish a DL-based Hierarchical CNN (H-CNN) for PC detection. Besides, the H-CNN training and configurations purposes are established for the efficiency of the PC image segment.

The authors [15] executed a CNN approach utilizing ResNet-50 to differentiate among MCN and SCN.

Data augmentation is employed for improving the quality and size of trained datasets. Fine-tuned training methods can be employed by executing the pre-training method in transfer learning (TL) but trained chosen layers. In [16], the authors present a new Multi-modal Fusion and Calibration Network (MFCNet) for tumor segmentation dependent upon 3D PET-CT images. Primarily, a Multimodal Fusion Downsampling Block (MFDB) with the remaining design was

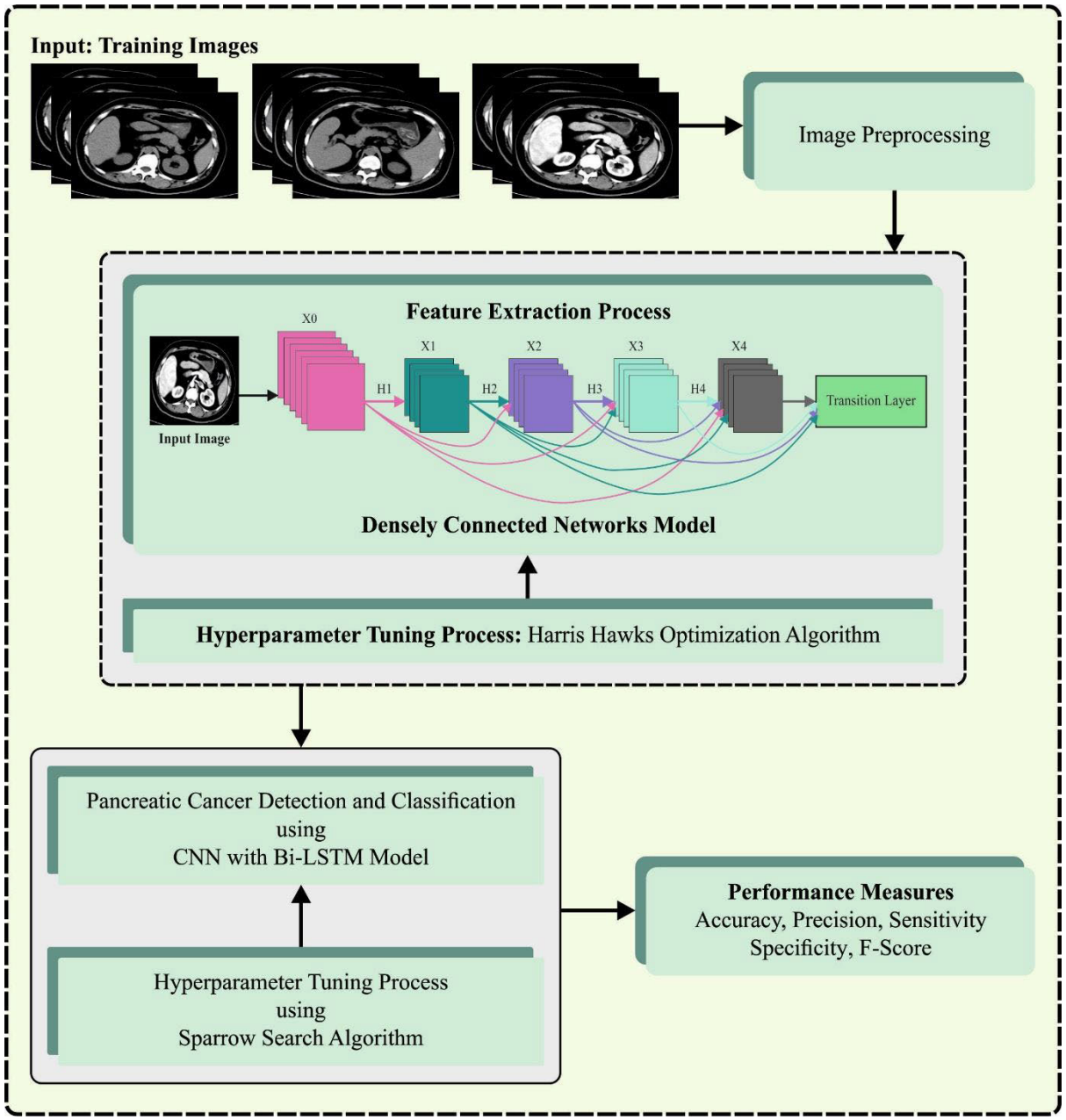

FIGURE 1. Workflow of SSASDL-PCDC algorithm.

presented. The presented MFDB fuse complementary feature of multimodal images but retained the single features of various modal images. Secondarily, the Multimodal Mutual Calibration Block (MMCB) dependent method of the inception infrastructure was planned.

Abbas and Obied [17] examine a CAD approach employing Synergic Inception ResNet-V2, Deep CNN structure for detection of PC cases in openly Usable CT images, which is removed PC graphical utility to contain medical analysis previously the pathogenic analysis, saving valued time for disease prevention. Liang et al. [18] purposes to establish a process enabling automatic segmentation of pancreatic GTV dependent upon multi-parametric MRI employing DNNs. The authors utilized a square-window-related CNN structure with 3 convolution layer blocks.

III. THE PROPOSED MODEL

In this study, we have established a novel SSASDL-PCDC approach for PC detection on CT images. The study aims to design an SSASDL-PCDC technique to achieve improved PC detection performance. The SSASDL-PCDC technique comprises several subprocesses such as DenseNet-based feature extraction, HHO-based hyperparameter tuning, CNN-BiLSTM-based classification, and SSA-based parameter optimization. Fig. 1 represents the workflow of the SSASDL-PCDC algorithm.

A. FEATURE EXTRACTION MODULE

In this work, the DenseNet121 approach was employed to derive features from the CT images. Huang et al. presented the DenseNet method, and this method improves feature reuse abilities dependent upon ResNet in their structure [19]. It takes $L(L+1)/2$ direct connections, but typical CNN takes L layers with L connections. In DenseNet, mapping features were integrated utilizing concatenation rather than summing previously passing as a layer, and every preceding layer mapping feature was employed as input to some particular layers. The Dense Block is the key infrastructure of DenseNet, containing convolution layers. DenseNet-121 is the most variations of the DenseNet structure containing a 121-connected convolution layer with the last resultant layer.

DenseNet-121 comprises 4 dense blocks, and there exists a transition layer among all the dense blocks. This network dense connectivity for $x0$, $x1$, $xl-1$ inputs, whereas the l^{th} layer obtains mapping features in every prior layer demonstrated as $Xl = Hl([x0,x1,\ldots,xl-1])$. Hl denotes the composite function which comprises 3 functions 3×3 convolutional, BN, and ReLU. All the dense blocks of DenseNet121 take 2 convolutional layers, 1×1 and 3×3 that are repeated differently from all the blocks. A transition layer comprises 1×1 convolution sand average pooling layers with a stride of 2. Previously sending every mapping feature to the FC layer for classification, this network carries out a 7×7 global average pooling layer.

Data-driven AI model is represented by 3 basic elements: the data use, the parameter utilized for training them, and the structure of network use them. Any DL algorithm should achieve a good balance amongst these components to perform tasks with maximal efficiency. A group of primary parameters is utilized in different trials to confirm the design of the model, and the model performance was measured within every trial. Furthermore, there exists optimization concern related to enhancing network depth. Additionally, improper selection of hyperparameters might lead to the suboptimum result. The manual hyperparameter tuning for DenseNet is a laborious process. Subsequently, the hyperparameter optimization algorithm should be implemented to iteratively find the optimum value dependent upon the trained data and upgrade them. The HHO is a metaheuristic optimizer algorithm utilized for the DenseHHO architecture. HHO is stimulated by the hunting behaviors of Harris hawks [20]. The HHO technique can resolve the problems of different optimization techniques namely parameter optimization, function optimization, and feature selection for ML algorithms. The subsequent steps need to be taken for implementing the algorithm. The most important variance among HHO and other optimizer techniques lies in the establishment of the concept of elite and non-elite hawks rather than following a severe hierarchical system. Consequently, elite hawk takes the lead in the search technique, which represents the best solution. It is mimic the behaviors of optimum hawks from the population to maintain their location. Thus, the algorithm could converge towards a potential solution using this exploitation process. These 3 kinds of hunting behaviors can be detected in Harris hawks:

- Exploration: Harris hawks randomly fly to determine novel regions where they could be searched.
- Exploitation: Harris Hawks attempts to enhance the solution given by the individual.
- Intensification: Harris hawks co-ordinate their effort to find their prey.

The HHO will be used to enhance the network hyperparameter after the initialization of the pre-trained module. The HHO exploits the following hunting behaviors to search for an optimum solution:

$$X_i^{t+1} = X_i^t + rand().\left(X_j^t - X_k^t\right), \tag{1}$$

In Eq. (1), $rand()$ denotes the random integer within [0, 1], j and k are two random selection hawks, and t shows the existing iteration. The Harris hawks guide the optimizer technique by updating the position according to the other hawks:

$$X_i^{f+1} = \frac{\left(X_i^t\right) + \left(X_j^t\right)}{2} + rand\ () \cdot \left(X_j^t - X_k^t\right), \tag{2}$$

B. DETECTION MODULE

For the detection and classification of PC, the CNN-BiLSTM model is used. The CNN, a conventional DNN, has fully connected, convolutional, and pooling layers [21]. It dynamically identifies the higher-level feature demonstration of time sequences in the multivariate time series prediction to gather considerable data and implements a local connection and global sharing for time sequences by the convolutional function. CNN is capable of analyzing the relationship between the variables accurately. Usually, the $1D$-CNN layer simplifies and improves the predictive model.

Here, a stacked BLSTM network was used as a basic element of the model that provides the advantage of capturing temporal data from different sequences. The data from the past and future time series are crucial to making forecasts on the $PV's$ power. Consequently, the bi-directional data in the PV correlation datasets was maximized by the BLSTM to discover the relationships between past, present, and future time steps. BLSTM is a development of the LSTM, an RNN variant which could resolve the vanishing gradient problem by integrating a pass-selective model. The context data can be attained from the previous statement of whole inputs; the BLSTM incorporates the past weather data in both ways and operated as follows:

$$\begin{aligned} f_t &= \sigma\left(W_f \times [h_{t-1}x_t] + b_f\right) \\ i_t &= \sigma\left(W_j \times [h_{t-1}x_t] + b_i\right) \\ \tilde{C}_t &= \tanh\left(W_C \times [h_{t-1}x_t] + b_C\right) \\ C_t &= f_t \times C_{t-1} + i_t \times \tilde{C}_t \end{aligned}$$

$$0_t = \sigma\left(W_0 \times [h_{t-1} x_t] + b_0\right)$$
$$h_t = 0_t \times tanh\left(C\right) \tag{3}$$

where h_{t-1} indicates the implicit layer state at the prior time; x_t denotes the input parameter at t moment , $\tilde{C}_t$ shows the temporary memory state at t time, C_{t-1} shows the unit memory layer from the prior instant; W and b embodies the weighted and biased utilized during the trained process and, and $f_t, i_t, 0_t$ represent the manages the amount of data generated by the forget gate, update gate, and memory units.

$$\vec{h}_t = \overrightarrow{LSTM}\left(h_{t-1}, x_t, c_{t-1}\right), t \in [1,T]$$
$$\overleftarrow{h}_t = \overrightarrow{LSTM}\left(h_{t+1}, x_t, c_{t+1}\right), t \in [T,1]$$
$$H_t = \left[\vec{h}_t, \overleftarrow{h}_t\right] \tag{4}$$

In Eq. (4), $\vec{h}_t$ shows the hidden layer of the forward layer at t time , $\overleftarrow{h}_t$ denotes the hidden layer of backward at t moment, and H_t represents the hidden state in the BLSTM for the t moment . Fig. 2 illustrates the framework of BiLSTM.

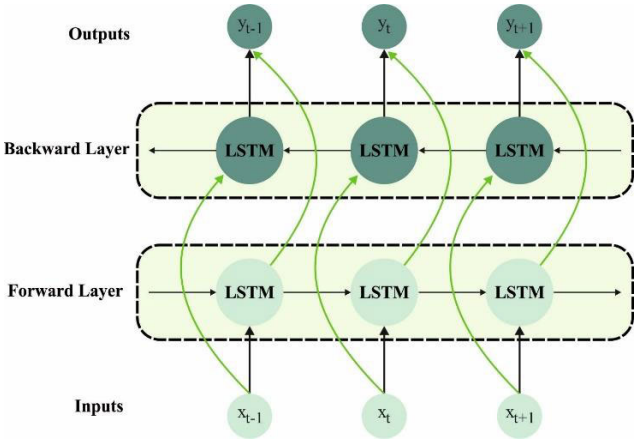

FIGURE 2. Architecture of BiLSTM.

C. HYPERPARAMETER TUNING MODULE

Finally, the SSA adjusts the hyperparameter values of the CNN-BiLSTM model. The high search efficiency and simple implementation of the SSA technique make it an intelligent optimization algorithm [22]. This approach splits the sparrow population as to finders and joiners, with finders seeking food and if food places for another joiner and groups searching by subsequent finders. Consider that the sparrow population comprises the size of parameters that enhanced d and n sparrows. The location matrix X characterizes the n sparrows in d-dimension space and is represented as follows:

$$X = \begin{bmatrix} x_1^1 & x_1^2 & \cdots & x_1^d \\ x_2^1 & x_2^2 & \cdots & x_2^d \\ \vdots & \vdots & \vdots & \vdots \\ x_n^1 & x_n^2 & \cdots & x_n^d \end{bmatrix} G_x = \begin{bmatrix} g\left(\left[x_1^1 \; x_1^2 \; \cdots \; x_1^d\right]\right) \\ g\left(\left[x_2^1 \; x_2^2 \; \cdots \; x_2^d\right]\right) \\ \vdots \\ g\left(\left[x_n^1 \; x_n^2 \; \cdots \; x_n^d\right]\right) \end{bmatrix} \tag{5}$$

In Eq. (5), n shows the sparrow counts, d denotes the dimensional of the variable being optimizer, χ represents the separate sparrows, and the value of all the rows in G_x shows the fitness value (FV) of individuals.

The joiners need a massive predation range to search for the best food, hence in all the iterations, the location of joiners is upgraded as:

$$X_{i,j}^{iter+1} = \begin{cases} X_{i,j} \cdot exp\left(-\dfrac{i}{\alpha \cdot iier_{\max}}\right) & R_2 < ST \\ X_{i,j} + QL & R_2 \geq ST \end{cases} \tag{6}$$

In Eq. (6), $iter_{\max}$ is the constant representing the maximal amount of iterations and $iter$ shows the existing iteration. α represents the random integer in the [0, 1]. $X_{i,j}$ refers to the value of j^{th} parameter of the i^{th} sparrows at t^{th} iterations. R_2 and ST denote the alarm value and safety threshold, correspondingly, L shows the matrix of dimension $1 \times d$, but all the elements are fixed as 1. If $R_2 \geq ST$, there exists danger; if $R_2 < ST$, the surroundings are safe and the finders search, and the population leaves flies and food toward other safer regions.

Joiners search for food by following and monitoring the modified finders, and once the lesser changed joiner could not obtain food, it creates a position alter to obtain additional food:

$$X_{i,j}^{iter+1} = \begin{cases} Q \cdot exp\left(\dfrac{x_{worst} - x_{i,i}^{iter}}{i^2}\right) & i > 2n \\ X_p^{iter+1} + \left|X_{i,j} - X_p^{iter+1}\right| A^+ L & otherwise \end{cases} \tag{7}$$

In Eq. (7), X_{worsi} signifies the worst location. X_p represents the fittest place presently occupied by the producer, *and* A refers to the matrix of $1 \times d$ size, where the element is assigned randomly both 1 and -1, and $A^+ = A^T(AA^T)^{-1}.i > n/2$ shows that i^{th} accession with lesser FVs is hungry and not able to search.

The initial position was generated randomly when the sparrow proportions that recognize danger reached 10-20% of the overall population. Then, the initialization joiners and finders involve in competition for food and upgrade the location still the maximal iteration counts are attained. At last, the sparrow with maximum global FV can be recognized as a global optimum performance:

$$X_{i,j}^{iter+1} = \begin{cases} X_{best}^{iter} + \beta \left|X_{i,j}^{iter} - X_{best}^{iter}\right| & f_i < f_g \\ X_{i,j}^{iter} + K \left|\dfrac{x_{i,j}^{iter} - X_{worst}^{iter}}{(f_i - f_w) + \varepsilon}\right| & f_i = f_g \end{cases} \tag{8}$$

In Eq. (8), X_{best} shows the present optimum location. K takes values within [1, 1]. In addition ε denotes a smaller constant utilized to avoid zero-division error. β denotes the step control parameter that is a randomly generated value with standard distribution with a mean of 0 and variance of 1.f_g and f_w indicate the present global optimum and worse FVs, correspondingly.

The SSA method progresses a fitness function (FF) for accomplishing greater classifier outcomes. It expresses a positive integer to archetypal the good solution for candidate performances. During this work, the minimized classifier error rate can be supposed to be FF, as depicted in Eq. (9).

$$fitness\,(x_i) = ClassifierErrorRate\,(x_i) = \frac{no.of\ misclassified\ instances}{Total\ no.of\ instances} * 100 \quad (9)$$

IV. RESULTS AND DISCUSSION

The pancreatic cancer classification results of the SSASDL-PCDC technique are tested using a CT image dataset, comprising 250 pancreatic tumor images and 250 non-pancreatic tumor images as defined in Table 1. Fig. 3 depicts the sample images.

TABLE 1. Details of database.

class	No. of Samples
Pancreatic Tumor	250
Non-Pancreatic Tumor	250
Total Samples	500

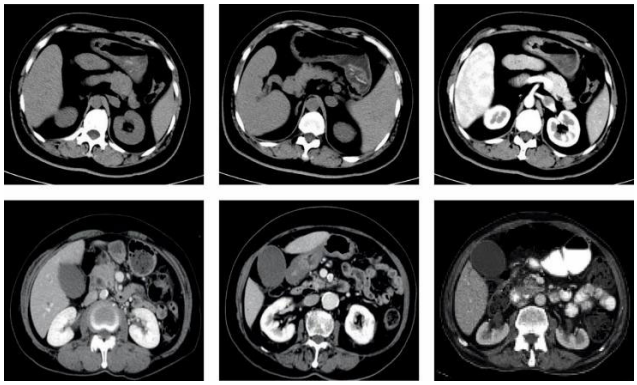

FIGURE 3. Sample images.

Fig. 4 showcases the classifier outcome of the SSASDL-PCDC approach under the test dataset. Fig. 4a portrays the confusion matrix presented by the SSASDL-PCDC system on 70% of TRP. The result implied that the SSASDL-PCDC algorithm has recognized 177 instances of Pancreatic Tumors and 166 instances of Non-Pancreatic Tumors. In addition, Fig. 4b represents the confusion matrix provided by the SSASDL-PCDC methodology on 30% of TSP. The outcome inferred that the SSASDL-PCDC algorithm has recognized 67 instances of Pancreatic Tumors and 82 instances of Non-Pancreatic Tumors. Followed by, Fig. 4c reveals the PR curve of the SSASDL-PCDC approach. The outcome stated that the SSASDL-PCDC system has achieved higher PR outcomes in 2 class labels. Lastly, Fig. 4d exemplifies the ROC curve of the SSASDL-PCDC algorithm. The result exhibited that the SSASDL-PCDC approach has resulted in capable outcomes with superior ROC values under 2 classes.

TABLE 2. Pancreatic cancer recognition outcome of SSASDL-PCDC approach on 70:30 TRP/TSP.

Class	$Accu_y$	$Prec_n$	$Sens_y$	$Spec_y$	F_{Score}
Training Phase (70%)					
Pancreatic Tumor	97.25	98.88	97.25	98.81	98.06
Non-Pancreatic Tumor	98.81	97.08	98.81	97.25	97.94
Average	98.03	97.98	98.03	98.03	98.00
Testing Phase (30%)					
Pancreatic Tumor	98.53	100.00	98.53	100.00	99.26
Non-Pancreatic Tumor	100.00	98.80	100.00	98.53	99.39
Average	99.26	99.40	99.26	99.26	99.33

TABLE 3. Comparative outcome of SSASDL-PCDC algorithm with other methods.

Methods	$Sens_y$	$Spec_y$	$Accu_y$
SSASDL-PCDC	99.26	99.26	99.26
IDLDMS-PTC [23]	99.05	98.84	99.15
ODL-PTNTC [24]	98.73	97.75	98.40
WELM Model [24]	97.76	97.67	97.26
KELM Algorithm [24]	96.66	97.53	96.69
ELM Algorithm [24]	96.27	97.27	96.21
CNN Model [25]	91.50	86.70	87.40

TABLE 4. CT outcome of SSASDL-PCDC algorithm with other methods.

Methods	Computational Time (sec)
SSASDL-PCDC	0.88
IDLDMS-PTC [23]	1.02
ODL-PTNTC [24]	1.37
WELM Model [24]	1.35
KELM Algorithm [24]	1.37
ELM Algorithm [24]	1.38
CNN Model [25]	1.48

In Table 2 and Fig. 5, an overall pancreatic cancer recognition result of the SSASDL-PCDC technique is displayed. The experimental values stated that the SSASDL-PCDC technique attains effectual recognition of pancreatic and non-pancreatic tumors. On 70% of TRP, the SSASDL-PCDC technique offers average $accu_y$, $prec_n$, $sens_y$, $spec_y$, and F_{score} of 98.03%, 97.98%, 98.03%, 98.03%, and 98% respectively. Meanwhile, on 30% of TSP, the SSASDL-PCDC algorithm provides average $accu_y$, $prec_n$, $sens_y$, $spec_y$, and F_{score} of 99.26%, 99.40%, 99.26%, 99.26%, and 99.33% correspondingly.

Fig. 6 displays the training accuracy TR_accu_y and VL_accu_y of the SSASDL-PCDC approach. The TL_accu_y

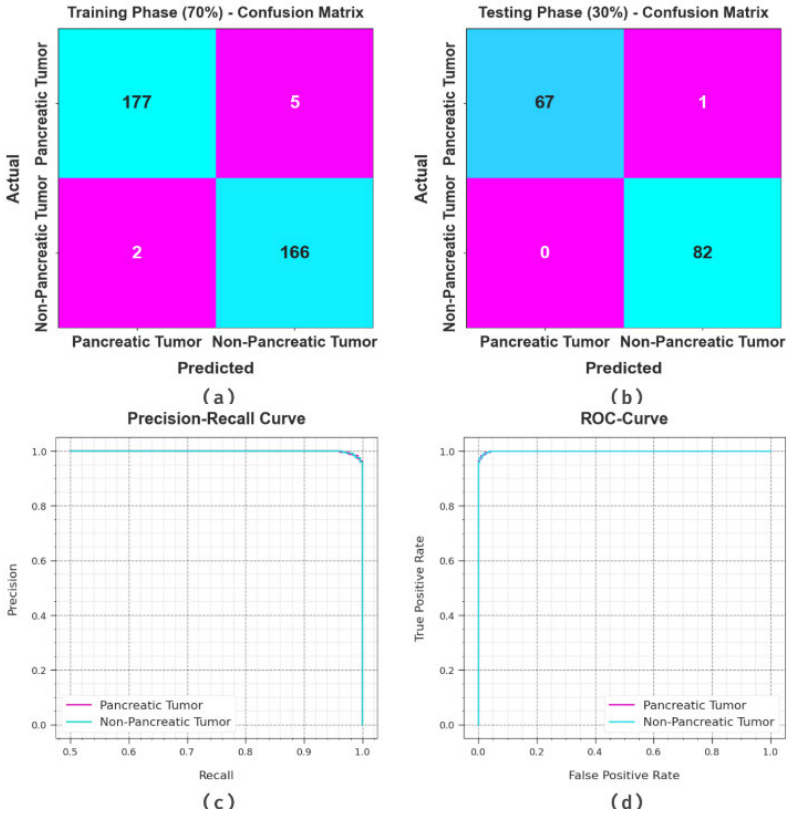

FIGURE 4. Performance of (a-b) Confusion matrices, (c) PR-curve, and (d) ROC curve.

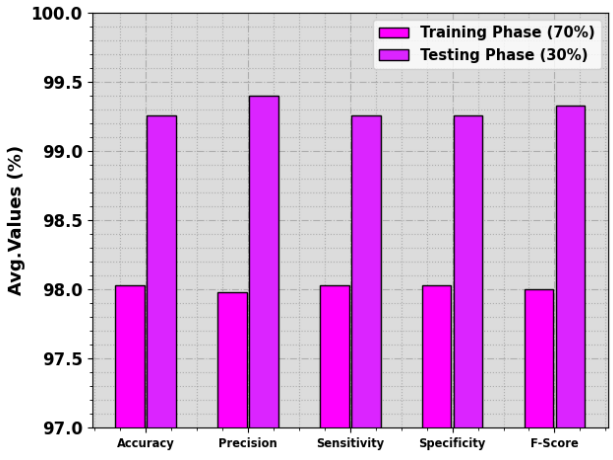

FIGURE 5. Average outcome of SSASDL-PCDC approach on 70:30 TRP/TSP.

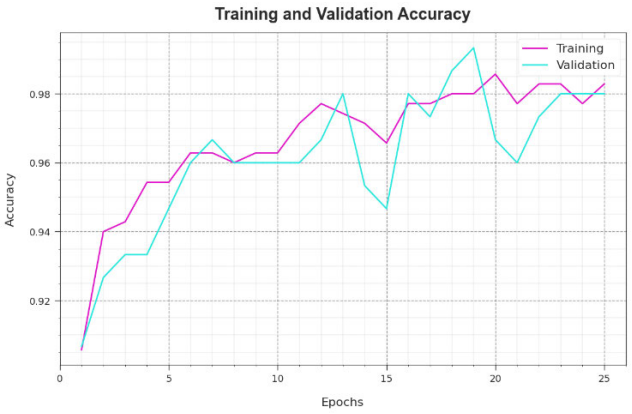

FIGURE 6. $Accu_y$ curve of the SSASDL-PCDC approach.

is defined by the estimate of the SSASDL-PCDC algorithm on the TR dataset whereas the VL_accu_y is computed by estimating the performance on a distinct testing dataset. The outcomes depict that TR_accu_y and VL_accu_y increase with an upsurge in epochs. Therefore, the performance of the SSASDL-PCDC approach obtains enhancement on the TR and TS dataset with an increase in the number of epochs.

In Fig. 7, the *TR_loss* and *VR_loss* outcomes of the SSASDL-PCDC algorithm are exposed. The *TR_loss* demonstrates the error among the predictive outcome and original values on the TR data. The *VR_loss* signifies the measure of the performance of the SSASDL-PCDC system on individual validation data. The outcomes inferred that the *TR_loss* and *VR_loss* incline to lesser with increasing epochs. It exposed the greater performance of the SSASDL-PCDC system and its capability to create a correct classification. The minimal value of *TR_loss* and *VR_loss* illustrates the greater outcome

of the SSASDL-PCDC approach to capturing patterns and relationships.

FIGURE 7. Loss curve of the SSASDL-PCDC approach.

Extensive comparative results of the SSASDL-PCDC technique are defined in Table 3 and Fig. 8 [23], [24], [25]. The result demonstrated that the CNN model reaches worse results whereas the WELM, KELM, and ELM models obtain slightly boosted performance. Along with that, the ODL-PTNTC model attains considerable performance. Next, the IDLDMS-PTC technique gains reasonable performance with $asens_y$ of 99.05%, $spec_y$ of 98.84%, and $accu_y$ of 99.15%. Nevertheless, the SSASDL-PCDC technique demonstrates maximum performance with $sens_y$ of 99.26%, $spec_y$ of 99.26%, and $accu_y$ of 99.26%.

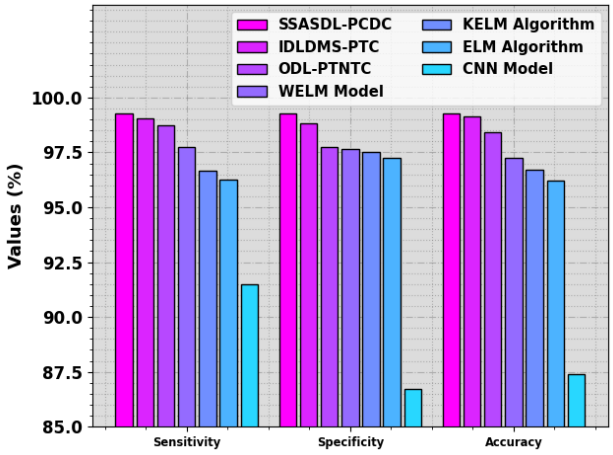

FIGURE 8. Comparative outcome of SSASDL-PCDC algorithm with other methods.

A brief CT analysis of the SSASDL-PCDC approach is described in Table 4 and Fig. 9. The outcome that outperformed the CNN approach obtains the least outcomes whereas the WELM, KELM, and ELM systems acquire somewhat boosted performances.

Followed by, the ODL-PTNTC method gains considerable results. Afterwards, the IDLDMS-PTC approach attains reasonable performance with a CT of 1.02s. Nevertheless, the

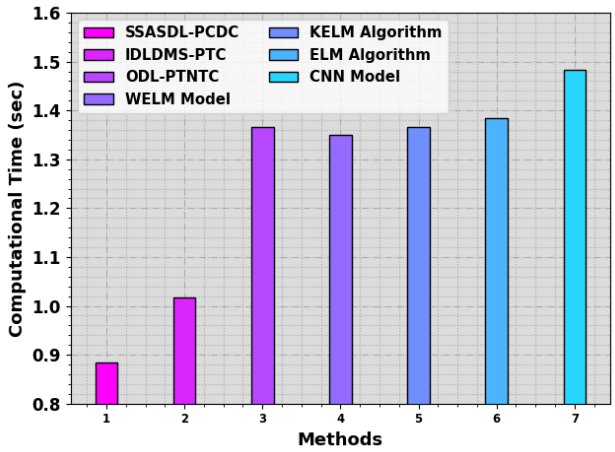

FIGURE 9. CT outcome of SSASDL-PCDC algorithm with other methods.

SSASDL-PCDC methodology displays lesser performance with a CT of 0.88s. Thus, the SSASDL-PCDC technique can be employed for accurate and automated pancreatic cancer classification.

V. CONCLUSION

In this study, we have established a novel SSASDL-PCDC system for PC detection on CT images. The study aims to design an SSASDL-PCDC technique to achieve improved PC detection performance. The SSASDL-PCDC technique comprises several subprocesses such as DenseNet-based feature extraction, HHO-based hyperparameter tuning, CNN-BiLSTM-based classification, and SSA-based parameter optimization. The SSA was utilized to adjust the hyperparameter values of the CNN-BiLSTM approach. To evaluate the effectiveness of the SSASDL-PCDC technique, extensive experiments were performed on a comprehensive dataset of pancreatic CT images. The experimental outcomes exhibit that the SSASDL-PCDC technique via integration of the SSA with stacked deep learning models significantly increases the accuracy of PC detection and classification. In future, the performance of the SSASDL-PCDC algorithm was increased by the employ of fusion-based approaches.

ACKNOWLEDGMENT

Princess Nourah bint Abdulrahman University Researchers Supporting Project number (PNURSP2023R300), Princess Nourah bint Abdulrahman University, Riyadh, Saudi Arabia.

REFERENCES

[1] S. Li, J. Xiao, L. He, X. Peng, and X. Yuan, "The tumor target segmentation of nasopharyngeal cancer in CT images based on deep learning methods," *Technol. Cancer Res. Treatment*, vol. 18, Jan. 2019, Art. no. 153303381988456.
[2] A. Gupta, A. Koul, and Y. Kumar, "Pancreatic cancer detection using machine and deep learning techniques," in *Proc. 2nd Int. Conf. Innov. Practices Technol. Manage. (ICIPTM)*, vol. 2, Feb. 2022, pp. 151–155.
[3] S.-L. Liu, S. Li, Y.-T. Guo, Y.-P. Zhou, Z.-D. Zhang, S. Li, and Y. Lu, "Establishment and application of an artificial intelligence diagnosis system for pancreatic cancer with a faster region-based convolutional neural network," *Chin. Med. J.*, vol. 132, no. 23, pp. 2795–2803, Dec. 2019.

[4] C. Song, M. Wang, Y. Luo, J. Chen, Z. Peng, Y. Wang, H. Zhang, Z.-P. Li, J. Shen, B. Huang, and S.-T. Feng, "Predicting the recurrence risk of pancreatic neuroendocrine neoplasms after radical resection using deep learning radiomics with preoperative computed tomography images," *Ann. Transl. Med.*, vol. 9, no. 10, p. 833, May 2021.

[5] M. N. M. Sehmi, M. F. A. Fauzi, W. S. H. M. W. Ahmad, and E. W. L. Chan, "Pancreatic cancer grading in pathological images using deep learning convolutional neural networks," *FResearch*, vol. 10, p. 1057, Nov. 2022.

[6] S.-H. Zhen, M. Cheng, Y.-B. Tao, Y.-F. Wang, S. Juengpanich, Z.-Y. Jiang, Y.-K. Jiang, Y.-Y. Yan, W. Lu, J.-M. Lue, J.-H. Qian, Z.-Y. Wu, J.-H. Sun, H. Lin, and X.-J. Cai, "Deep learning for accurate diagnosis of liver tumor based on magnetic resonance imaging and clinical data," *Frontiers Oncol.*, vol. 10, p. 680, May 2020.

[7] R. Yang, Y. Chen, G. Sa, K. Li, H. Hu, J. Zhou, Q. Guan, and F. Chen, "CT classification model of pancreatic serous cystic neoplasms and mucinous cystic neoplasms based on a deep neural network," *Abdominal Radiol.*, vol. 47, pp. 232–241, Oct. 2021.

[8] M. Kriegsmann, K. Kriegsmann, G. Steinbuss, C. Zgorzelski, A. Kraft, and M. M. Gaida, "Deep learning in pancreatic tissue: Identification of anatomical structures, pancreatic intraepithelial neoplasia, and ductal adenocarcinoma," *Int. J. Mol. Sci.*, vol. 22, no. 10, p. 5385, May 2021.

[9] A. B. Bagheri, M. D. Rouzi, N. A. Koohbanani, M. H. Mahoor, M. G. Finco, M. Lee, B. Najafi, and J. Chung, "Potential applications of artificial intelligence and machine learning on diagnosis, treatment, and outcome prediction to address health care disparities of chronic limb-threatening ischemia," *Seminars Vascular Surg.*, to be published, doi: 10.1053/j.semvascsurg.2023.06.003.

[10] C. Park, M. D. Rouzi, M. M. U. Atique, M. G. Finco, R. K. Mishra, G. Barba-Villalobos, E. Crossman, C. Amushie, J. Nguyen, C. Calarge, and B. Najafi, "Machine learning-based aggression detection in children with ADHD using sensor-based physical activity monitoring," *Sensors*, vol. 23, no. 10, p. 4949, May 2023.

[11] N. Alves, M. Schuurmans, G. Litjens, J. S. Bosma, J. Hermans, and H. Huisman, "Fully automatic deep learning framework for pancreatic ductal adenocarcinoma detection on computed tomography," *Cancers*, vol. 14, no. 2, p. 376, Jan. 2022.

[12] K. V. Chaithanyadas and G. R. G. King, "Detection of pancreatic tumor from computer tomography images using 3D convolutional neural network," in *Computational Vision and Bio-Inspired Computing* Singapore: Springer, 2023, pp. 289–303.

[13] K. Sekaran, P. Chandana, N. M. Krishna, and S. Kadry, "Deep learning convolutional neural network (CNN) with Gaussian mixture model for predicting pancreatic cancer," *Multimedia Tools Appl.*, vol. 79, nos. 15–16, pp. 10233–10247, Apr. 2020.

[14] W. Xuan and G. You, "Detection and diagnosis of pancreatic tumor using deep learning-based hierarchical convolutional neural network on the Internet of Medical Things platform," *Future Gener. Comput. Syst.*, vol. 111, pp. 132–142, Oct. 2020.

[15] L. S. Nguon, K. Seo, J.-H. Lim, T.-J. Song, S.-H. Cho, J.-S. Park, and S. Park, "Deep learning-based differentiation between mucinous cystic neoplasm and serous cystic neoplasm in the pancreas using endoscopic ultrasonography," *Diagnostics*, vol. 11, no. 6, p. 1052, Jun. 2021.

[16] F. Wang, C. Cheng, W. Cao, Z. Wu, H. Wang, W. Wei, Z. Yan, and Z. Liu, "MFCNet: A multi-modal fusion and calibration networks for 3D pancreas tumor segmentation on PET-CT images," *Comput. Biol. Med.*, vol. 155, Mar. 2023, Art. no. 106657.

[17] S. K. Abbas and R. S. Obied, "Novel computer aided diagnostic system using synergic deep learning technique for early detection of pancreatic cancer," *Webology*, vol. 18, no. 2, pp. 367–379, Oct. 2021.

[18] Y. Liang, D. Schott, Y. Zhang, Z. Wang, H. Nasief, E. Paulson, W. Hall, P. Knechtges, B. Erickson, and X. A. Li, "Auto-segmentation of pancreatic tumor in multi-parametric MRI using deep convolutional neural networks," *Radiotherapy Oncol.*, vol. 145, pp. 193–200, Apr. 2020.

[19] G. Huang, Z. Liu, L. Van Der Maaten, and K. Q. Weinberger, "Densely connected convolutional networks," in *Proc. IEEE Conf. Comput. Vis. Pattern Recognit. (CVPR)*, Jul. 2017, pp. 4700–4708.

[20] P. P. F. Rajeena, W. N. Ismail, and M. A. S. Ali, "A metaheuristic Harris hawks optimization algorithm for weed detection using drone images," *Appl. Sci.*, vol. 13, no. 12, p. 7083, Jun. 2023.

[21] L. Liu, K. Guo, J. Chen, L. Guo, C. Ke, J. Liang, and D. He, "A photovoltaic power prediction approach based on data decomposition and stacked deep learning model," *Electronics*, vol. 12, no. 13, p. 2764, Jun. 2023.

[22] J. Madiniyeti, Y. Chao, T. Li, H. Qi, and F. Wang, "Concrete dam deformation prediction model research based on SSA–LSTM," *Appl. Sci.*, vol. 13, no. 13, p. 7375, Jun. 2023.

[23] T. Vaiyapuri, A. K. Dutta, I. S. H. Punithavathi, P. Duraipandy, S. S. Alotaibi, H. Alsolai, A. Mohamed, and H. Mahgoub, "Intelligent deep-learning-enabled decision-making medical system for pancreatic tumor classification on CT images," *Healthcare*, vol. 10, no. 4, p. 677, 2022, doi: 10.3390/healthcare10040677.

[24] M. M. Althobaiti, A. Almulihi, A. A. Ashour, R. F. Mansour, and D. Gupta, "Design of optimal deep learning-based pancreatic tumor and nontumor classification model using computed tomography scans," *J. Healthcare Eng.*, vol. 2022, pp. 1–15, Jan. 2022.

[25] K.-L. Liu, T. Wu, P.-T. Chen, Y. M. Tsai, H. Roth, M.-S. Wu, W.-C. Liao, and W. Wang, "Deep learning to distinguish pancreatic cancer tissue from non-cancerous pancreatic tissue: A retrospective study with cross-racial external validation," *Lancet Digit. Health*, vol. 2, no. 6, pp. e303–e313, Jun. 2020.